Author Manuscript

Author Manuscript

Author Manuscript

Author Manuscript

HHS Public Access

Author manuscript

Neuroimage. Author manuscript; available in PMC 2017 March 01.

Published in final edited form as:

Neuroimage. 2016 March ; 128: 85–95. doi:10.1016/j.neuroimage.2015.12.032.

Effects of Magnetization Transfer on T_1 Contrast in Human Brain White Matter

Peter van Gelderen, **Xu Jiang**, and **Jeff H. Duyn***

Advanced MRI Section, Laboratory of Functional and Molecular Imaging, National Institutes of Neurological Disorders and Stroke, National Institutes of Health, Bethesda, Maryland 20892, USA

Abstract

MRI based on T_1 relaxation contrast is increasingly being used to study brain morphology and myelination. Although it provides for excellent distinction between the major tissue types of grey matter, white matter, and CSF, reproducible quantification of T_1 relaxation rates is difficult due to the complexity of the contrast mechanism and dependence on experimental details. In this work, we perform simulations and inversion-recovery MRI measurements at 3 T and 7 T to show that substantial measurement variability results from unintended and uncontrolled perturbation of the magnetization of MRI-invisible ^{1}H protons of lipids and macromolecules. This results in bi-exponential relaxation, with a fast component whose relative contribution under practical conditions can reach 20%. This phenomenon can strongly affect apparent relaxation rates, affect contrast between tissue types, and result in contrast variations over the brain. Based on this novel understanding, ways are proposed to minimize this experimental variability and its effect on T_1 contrast, quantification accuracy and reproducibility.

Keywords

brain tissue; white matter; myelin; T_1*contrast*; magnetization transfer; macro-molecular content

INTRODUCTION

Longitudinal proton relaxation (also called T_1 relaxation) is one of the major MRI contrast mechanism used for studying brain morphology, and is widely used for clinical diagnosis. Resulting from the magnetic interaction of protons with their environment, it is dependent on tissue composition and structure, including the local concentration of proteins and lipids. Additional, and sometimes strong contributions may come from atoms and molecules with para- and ferromagnetic properties such as endogenous iron and deoxyhemoglobin, or injected contrast agents such as Gd-DTPA and Feridex.

*Corresponding author: Tel: 301-594-7305, jhd@helix.nih.gov.

Publisher's Disclaimer: This is a PDF file of an unedited manuscript that has been accepted for publication. As a service to our customers we are providing this early version of the manuscript. The manuscript will undergo copyediting, typesetting, and review of the resulting proof before it is published in its final citable form. Please note that during the production process errors may be discovered which could affect the content, and all legal disclaimers that apply to the journal pertain.

Author Manuscript Author Manuscript Author Manuscript Author Manuscript

T_1-weighted MRI techniques such as MP-RAGE (Mugler and Brookeman 1990) and inversion recovery (IR) fast spin echo (see e.g. (Clark, Courchesne et al. 1992, Constable, Smith et al. 1992, Smith, Constable et al. 1994, Zhu and Penn 2005, Barazany and Assaf 2012)), both of which are based on signal recovery after instantaneous magnetization inversion, are being extensively used for the distinction between brain tissue types, including the segmentation of grey matter, white matter, and CSF. The distinctly different T_1 relaxation between grey and white matter has been attributed on their different myelin content: myelin rich white matter contains an up to 30% fraction of proteins and lipids (Randall 1938), whose largely invisible hydrogen (^{1}H) protons exhibit rapid T_1 relaxation (Deese, Dratz et al. 1982, Ellena, Hutton et al. 1985, Du, Sheth et al. 2014) and, through magnetization transfer, accelerate T_1 relaxation of MRI visible water ^{1}H protons (WP's). Thus, study of T_1 relaxation with inversion recovery may allow quantification of this magnetization transfer (MT) (Edzes and Samulski 1977, Gochberg and Gore 2003, Dortch, Moore et al. 2013) and aid in determining brain myelin content (Stuber, Morawski et al. 2014), which has important neuro-scientific and clinical applications (Dinse, Waehnert et al. 2013). MRI techniques such as MP2RAGE (Van Gelderen, Koretsky et al. 2006, Marques, Kober et al. 2010) and DESPOT1 (Deoni, Rutt et al. 2008) have recently been proposed and are increasingly being used for this purpose (Dinse, Hartwich et al. 2015). One of the outstanding issues with quantification of the T_1 time constant is the limited reproducibility of the various methods and the variation in T_1 estimates reported in literature (see e.g. (Labadie, Lee et al. 2014, Stikov, Boudreau et al. 2015)). While incompletely understood, this variability can be partly attributed to imperfect WP inversion, and a potential bi-exponential character of the relaxation that is not properly accounted for during analysis (Kingsley, Ogg et al. 1998, Barral, Gudmundson et al. 2010, Labadie, Lee et al. 2014, Stikov, Boudreau et al. 2015). As a result, generalizability of T_1 quantification results is rather limited, hampering the study of brain myelination, and affecting the accuracy of tissue segmentation.

The goal of the current work was to investigate the presence of bi-exponential longitudinal relaxation in human brain and its dependence on experimental parameters, including inversion pulse type and magnetic field strength. For this purpose, dedicated IR experiments were performed at 3 T and 7 T, as well as MT experiments in which non-water ^{1}H protons were selectively saturated by replacing the inversion pulse by an MT pulse. Conjoint analysis using a two-pool model of MT showed that in white matter, T_1 relaxation is strongly dependent on the effect of the inversion pulse not only on WPs, but also on the non-water ^{1}H protons. In addition, we provide realistic estimates for the T_1 of these protons, an essential parameter for the interpretation and quantification of T_1 and MT data.

METHODS

Background

Myelin is an important contributor to T_1 contrast between brain regions (Koenig, Brown et al. 1990). The mechanistic interpretation has been that ^{1}H protons on larger molecules (such as the proteins and lipids that are abundant in myelin) have short T_1 and this affects the T_1 of WPs by means of MT through mechanisms such as dipolar coupling and chemical exchange.

Author Manuscript Author Manuscript Author Manuscript Author Manuscript

This notion is corroborated by the fact that, in human brain, the relaxation rate R_1 (=1/T_1) strongly correlates with (semi) solid (i.e. non-water) fraction (Fatouros, Marmarou et al. 1991, Fatouros and Marmarou 1999, Rooney, Johnson et al. 2007). Similarly, study of MT effects with experiments that selectively affect (i.e. saturate) the (semi) solid proton fraction (from here onwards categorically, but somewhat incorrectly, indicated by macromolecular proton fraction, or MP fraction) have found a dominant effect in myelinated tissue, and such experiments have been used to measure myelin loss in diseases such as MS. Thus, MT is an important mechanism underlying T_1 relaxation in the human brain.

Study of T_1 relaxation *in-vivo* is typically performed with IR-type experiments (of which MPRAGE is an example) that measure recovery of the longitudinal magnetization (indicated with *M(t)*) at one or more time-point(s) *t* after inversion of the WP magnetization by a radiofrequency (RF) inversion pulse. In pure liquids with only one species of ^{1}H, *M(t)* can generally be described by a single exponential function, characterized by time constant T_1. For the more complex situation of brain tissue, it has been suggested that *M(t)* can be approximated by using a two-pool model of MT between WP and MP, which leads to bi-exponential behavior (Zimmerman and Britten 1957, Gochberg, Kennan et al. 1997, Prantner, Bretthorst et al. 2008, Labadie, Lee et al. 2014):

$$S_{WP}(t)=1-\frac{M_{WP}(t)}{M_{WP}(\infty)}=a_1e^{-\lambda_1 t}+a_2e^{-\lambda_2 t} \quad [1]$$

$$2\lambda_{1,2}=R_{1,WP}+R_{1,MP}+k_{MW}+k_{WM}\pm\sqrt{(R_{1,WP}-R_{1,WP}+k_{MW}-k_{WM})^2+4k_{MW}k_{WM}} \quad [2]$$

$$a_{1,2}=\pm\frac{S_{WP}(0)(R_{1,WP}+k_{WM}-\lambda_{2,1})-S_{MP}(0)k_{WM}}{\lambda_1-\lambda_2} \quad [3]$$

$$(1-f)k_{WM}=fk_{MW} \quad [4]$$

Here, *M(t)* is converted to fractional saturation *S(t)*, which can range from 0–2. Indices WP and MP refer to water protons and macromolecular protons respectively. The fast (λ_1) and slow (λ_2) rate constants are determined by the intrinsic relaxation and exchange rates of the tissue, while the amplitudes (a_1 and a_2) depend on the conditions of the experiment, including the properties of the RF pulse. These equations broadly apply to any type of RF pulse, including imperfect inversions or MT pulses that selectively saturate the MP pool. The first order MT rate constants from WP to MP and *vice versa* are given by k_{WM} and k_{MW} respectively; these relate through the MP pool fraction *f* according to Eq. 4 (Because of this relation between the exchange rates, the model can be equivalently be described in terms of one of the two rate constants (*k*) and the MP-pool fraction (*f*)). $R_{1,WP}$ and $R_{1,MP}$ are relaxation rates in absence of exchange.

Importantly, the amplitudes of the two exponential functions (a_1 and a_2) are not only dependent on the effect of the RF pulse on WP, but also on MP. Because the latter (i.e. $S_{MP}(0)$) is difficult to estimate (S_{MP} is not directly visible), previous work has used

Author Manuscript Author Manuscript Author Manuscript Author Manuscript

simplifying assumptions equating $S_{MP}(0)$ to either 1 (Gochberg, Kennan et al. 1999) or 0 (Wilhelm, Ong et al. 2012). In the following, we will show that under practical conditions, the actual value of $S_{MP}(0)$ can differ substantially from these values, and demonstrate the effect of $S_{MP}(0)$ on the bi-exponential nature of the recovery curve. For this purpose, estimates of $S_{MP}(0)$ were derived from joint analysis of recovery curves obtained with four different inversion pulses and one MT-type RF pulse (the latter referred to as "MT data"), as detailed in the next section. Qualitative estimates were also derived from simulations of the MT and inversion pulses with numerical solution of the Bloch equations (see section "simulations" below).

Estimating $S_{MP}(0)$ experimentally

While λ_1, λ_2, a_1, a_2 can be directly determined from fitting of $S_{MP}(t)$in Eq. (1) to IR or MT data, estimation of $S_{MP}(0)$ requires subsequently solving Eqs. (2) and (3), which represent 4 equations with the 6 unkowns: $S_{WP}(0)$, $S_{MP}(0)$, $R_{1,MP}$, $R_{1,WP}$, k_{WM}, and k_{MW}. To resolve this, at least two constraints need to be added to the system of equations. Here, this was done in a two-pronged, sequential analysis approach: 1) A voxel-wise analysis was performed which assumed $R_{1,MP}$ and $R_{1,WP}$ to be constant across the brain and determined their approximate values by constraining $S_{MP}(0)$ to have realistic values for both IR and MT data; 2) Then a region-of-interest (ROI) analysis was performed which used $R_{1,MP}$ found from the global analysis and fine-tuned $R_{1,WP}$ using assumed $S_{MP}(0)$ for the MT data, and then accurately determined $S_{MP}(0)$ for the four different inversion pulses. Further details are provided below under "data analysis".

The rationale for assuming constant $R_{1,MP}$ and $R_{1,WP}$ is based on the above-mentioned the notion that in WM, the dominant source of T_1 contrast are variations in f , with the two having a close to linear relationship (Koenig, Brown et al. 1990, Fatouros and Marmarou 1999, Gelman, Ewing et al. 2001, Rooney, Johnson et al. 2007, Helms and Hagberg 2009, Mezer, Yeatman et al. 2013, Callaghan, Helms et al. 2015)

MRI measurements

Ten subjects participated in this study (ages 19–60, average 30.4, 6 female), after consenting into an IRB approved protocol. Subjects were scanned at both 3 T and 7 T scanners (Siemens, Erlangen, Germany; Skyra and Magnetom platforms respectively) using 32-channel receive arrays.

IR measurements were performed using and adiabatic pulse and 3 different composite pulses. The adiabatic pulse (indicated by 'A5.1') was a commonly used hyperbolic secant of 5.12 ms duration, 0.51 $(\mu T)^2$s energy, a B_1 modulation frequency of 833 Hz and a β of 1400 s^{-1} (Tannus and Garwood 1997); for optimal inversion efficiency, its amplitude was adjusted to smoothly start and end at zero. The three composite inversion pulses (90^0_x-180^0_y-90^0_x) were designed to lead to different levels of $S_{MP}(0)$ by varying their energy. For this purpose, pulse duration was varied between 1.2, 3.6 and 6.9 ms (pulses indicated by 'C1.2','C3.6' and 'C6.9' respectively; corresponding B_1's: 833, 278 and 145Hz, energies: 0.46, 0.15, and 0.08 $(\mu T)^2$s). The MT pulse consisted of a train of 16 hard

Author Manuscript Author Manuscript Author Manuscript Author Manuscript

pulses with angles 60°, -120°, 120°, -120°, ….120°,-60°, a total length of 6 ms and a B_1 amplitude of 833 Hz.

Image data were acquired with single-shot EPI, sampling 5 slices consecutively after each RF inversion or MT pulse; cycling the slice order over 5 repetitions thus resulted in acquisition of 5 delay times for each slice (Ordidge, Gibbs et al. 1990). Slices of 2 mm thickness were placed with 1.5 mm separation parallel to AC-PC line and encompassed the central part of the corpus callosum. The inversion delay (TI) values were 9, 71, 147, 283 and 1200 ms at 3 T and 7, 64, 145, 283 and 1200 ms at 7 T (defined as the time from the center of the inversion pulse to the center of the EPI excitation pulse). The delay times for the MT experiments were: 10, 72, 138, 258 and 600 ms for 3 T, and 8, 62, 137, 256 and 600 ms for 7 T. The times were chosen to preferentially sample the early part of the IR curve, within the constraint of the minimal slice TR set by the duration of the EPI readout. The image resolution was 144x108 with SENSE rate-2 acceleration, the field-of-view was 240x180mm. The echo time (TE) was 30 ms at 3 T and 24 ms at 7 T, the TR 4 s for the inversion experiments, and 3 s for the MT experiment. In order to suppress signals from scalp lipids, the TE was increased on even numbered repetitions. This increase amounted to 1.15 and 0.48 ms for 3 T and 7T respectively, resulting in a phase inversion of the lipid signal with respect to water (assuming a 3.5 ppm frequency difference between lipid and water). Summation of odd and even numbered images thus resulted in cancellation of lipid signal. Fourteen repetitions were acquired at 3 T and 18 at 7 T, the first 4 of which omitted the inversion (or MT) pulse and used to provide a reference signal to estimate M_{WP} (∞) in Eq. 1, and allow conversion of the measured signals to saturation levels ($S_{WP}(t)$).

Data Analysis

Pre-processing—Pre-processing included motion correction, averaging, polarity correction, and calculation of signal saturation levels. Prior to averaging repetitions, complex images were spatially registered to correct for motion. Only in-plane registration was performed, as the small number of slices did not support through-plane motion correction. For the inversion data, polarity correction was applied to the magnitude signal based on the phase difference with the (un-inverted) reference image. This was a largely automatic procedure, however, in a small number of voxels manual signal polarity adjustment was required for the longest TI. The fractional magnetization level expressed in Eq. 1 was determined by dividing each inversion image by the corresponding reference image (i.e. data acquired without inversion pulse). This was done for all voxels where the reference signal exceeded 5% of maximum. Analogous analysis was performed for the MT data, however without performing the signal polarity adjustment. All processing was done in IDL (Exelsis Visual Information Solutions, Boulder, CO, USA).

Voxel-wise analysis—To derive estimates for $R_{1,WP}$ and $R_{1,MP}$, data from a single IR experiment (using the adiabatic pulse) was analyzed jointly with the MT data on a voxel-wise basis (Fig. 1). This was done for both field strengths and involved the following steps:

1. Jointly fit MT and IR data to Eq. 1, yielding one pair of decay rates (λ_1, λ_2) and two pairs of amplitudes (a_1, a_2) for each voxel.

Author Manuscript Author Manuscript Author Manuscript Author Manuscript

2. Assuming global values for $R_{1,WP}$ and $R_{1,MP}$, calculate corresponding levels of $S_{MP}(0)$ for IR and MT experiments for each voxel, based on decay rates and amplitudes found in step 1.
3. Adjust $R_{1,WP}$ and $R_{1,MP}$ and recalculate $S_{MP}(0)$ to maximize the number of voxels with $S_{MP}(0)$ values consistent with predetermined constraints.

The constraints for step 3 were as follows: a) $S_{MP}(0)<1$ for both IR and MT data (MP can not be inverted due to their short T_2) , b) based on the pulse durations and energy (6.0 resp. 5.1ms, 2.3 resp. 0.51 $(\mu T)^2 s$), the ratio of $S_{MP}(0)$ for the adiabatic inversion pulse and the MT pulse is between 0.7 and 1.0 as determined from simulations (details below and in Fig. 3a and c).

ROI-based analysis—ROI analysis was performed on all datasets in order to fine-tune $R_{1,WP}$ and calculate $S_{MP}(0)$ for each of the four inversion pulses (Fig. 2). For this purpose, in each subject, a WM ROI in the splenium of the corpus callosum was selected manually, and $R_{1,MP}$ was set to the value found by the voxel-wise analysis. Furthermore $S_{MP}(0)$ values for the MT pulse were set to 0.88 and 0.92 for 3 T and 7 T respectively, based on previous measurements that investigated $S_{MP}(0)$ dependence on MT pulse length. The rationale for fine-tuning $R_{1,WP}$ based on assumed levels of $S_{MP}(0)$ for the MT experiment was that the latter was relatively well known, compared to the significant uncertainty in $R_{1,WP}$ found in the voxel-wise analysis.

The ROI-based analysis involved the following steps:

1. Jointly fit MT and IR data to Eq. (1), yielding one pair of decay rates (λ_1, λ_2) and five pairs of amplitudes (a_1, a_2).
2. Using the fixed values for $R_{1,MP}$, and $S_{MP}(0)$ for the MT data, as well as the decay rates and MT amplitudes from step 1, calculate $R_{1,WP}$ and MT rates (k_{WM} and k_{MW}).
3. Calculate $S_{MP}(0)$ for each of the four inversion experiments using their specific pairs of amplitudes. Finally, in order to estimate reproducibility, for each fitted parameter, the standard deviation (SD) over subjects was calculated.

Simulations

Simulations were performed to study the various aspects of the experiment, including the effects of the IR and MT pulses on $S_{WP}(0)$ *and* $S_{MP}(0)$, the effect of $S_{MP}(0)$ on the IR signal trajectory, the effect of noise and finite TR on parameter fitting. All simulations were performed in IDL.

Effect of inversion and MT pulses on $S_{WP}(0)$ and $S_{MP}(0)$—Simulations of the effects of the inversion and MT pulses on $S_{WP}(0)$ and $S_{MP}(0)$ were based on the Bloch equations and investigated dependence on T_2 , assuming single exponential T_2 decay. For this purpose, temporal evolution was discretized using 1 μs time steps, and the evolution of the three Cartesian components of the magnetization was effectuated by successively applying rotations and multiplications to represent effects of the RF pulse and T_2 decay

Author Manuscript Author Manuscript Author Manuscript Author Manuscript

respectively. One hundred different T_2 values were used, exponentially distributed between 1 μs and 1 s. In a second simulation, pulse length of the composite inversion pulse was varied (and as a result its energy) at a single T_2 (70 μs, in the estimated range of MP), to illustrate the effect on $S_{MP}(0)$. Exchange was ignored in both simulations, as the applied RF pulses are short compared to the relevant exchange rates. A Lorentzian line shape (implicit in the exponential solution to the time domain Bloch equations) was used for three reasons: a) calculations with different line-shapes requires treatment in the spectral domain, which implies linearity of the system, an assumption that is applicable for small tip-angles experiments but not necessarily for inversions and/or short, high-power MT pulses; b) it has been suggested that in myelin, MP may exhibit a Lorentzian lineshape (Horch, Gore et al. 2011) with a T_2 in 60–100μs range; c) this simulation is meant as a general illustration of the pulse effects, not as an exact study of MP T_2 values and line shapes, and it can be reasonably assumed different line-shape models would show similar trends as function of pulse power.

The effect of $S_{MP}(0)$ on the IR signal trajectory—To investigate the effect of $S_{MP}(0)$ on T_1 relaxation, the magnetization trajectory of the two pools in the IR experiment was simulated using the two-pool model equations (Eq. [1–4]) and the parameters found from fitting of the experimental data obtained at 7 T. Two extreme cases were simulated: one with complete saturation of the MP pool ($S_{MP}(0)$= 1.0) and one without any saturation ($S_{MP}(0)$= 0.0), while the WP pool was assumed to be perfectly inverted in both cases ($S_{WP}(0)$= 2.0). This simulation was run for both field strengths separately, as the $R_{1,MP}$ was found to be field dependent. From this data, the relative contribution of the rapidly relaxing component (rate λ_1) to the IR curve was estimated and a TI value was extracted above which its contribution becomes negligible. This was done by calculating the instantaneous T_1 (from $-S(t)/(dS(t)/dt)$) and ascertain when this reaches 95% of its long TI limit value, which is the inverse of the slow component rate (λ_2).

The effect of noise and finite TR on parameter fitting—To gain some insight into the stability of the two-pool model fitting procedure under influence of noise, noise was added to a synthetic signal recovery curve (using Eq. (1)) generated based on subject averaged model parameters extracted with the ROI-based fitting procedure (Table 2). The noise level was determined from the experimentally determined ROI-based fitting residue and corresponded to a SNR of 500:1 in the ROI-averaged signal. After each of 100,000 realizations of noise addition, the data was subjected to the ROI-based fitting procedure (Fig. 2), after which the SD of the extracted parameters was determined.

To investigate the influence of the finite TR and incomplete magnetization recovery between scan repetitions on the extracted parameters, the evolution of the magnetization in the IR and MT experiments was simulated, again based on the experimentally determined two-pool model parameters (k, f, and R in Table 2). This was done both for the actual TRs used in the experiments (4 s and 3 s for IR and MT) respectively), as well as for a TR of 12 s at which complete recovery was assumed. Both conditions were subjected to the ROI-based fitting procedure and the resulting parameter values were compared.

Author Manuscript Author Manuscript Author Manuscript Author Manuscript

RESULTS

Initial evaluation of the effect of inversion pulse type on T_1 relaxation was performed with simulations. Fig. 3a shows the effect of the each of the experimentally used inversion pulses on M as a function of T_2. While all inversion pulses nearly fully invert the long T_2 WP ($T_2 >$ 20 ms), a highly variable saturation is observed for T_2 values typical of MP (60–100 μs for Lorentzian lineshape, which has linewidth equivalent to 10–15 μs Superlorentzian). The increasing saturation of MP (i.e. $S_{MP}(0)$) with decreasing inversion pulse duration is attributed to the increased pulse energy (Fig. 3b). The T_2 dependence of the saturation efficiency of the MT pulse (Fig. 3c) indicates almost complete saturation for MP and negligible saturation for WP. Simulation of the effect of variable MP saturation of the inversion pulse on IR characteristics shows an increasingly bi-exponential recovery with reduced MP saturation (Fig. 3d). As a result, a relatively high relaxation rate at the initial part of the recovery curve is observed.

Results of the experimental investigation into the effect of inversion pulse characteristics on T_1 relaxation are summarized Figs. 4–6, and Tables 1 and 2. In brief, a bi-exponential recovery is observed that is dependent on pulse type, consistent with the notion that increasing pulse energy leads to a higher $S_{MP}(0)$. As illustrated in Fig. 4, following WP inversion, the initial (apparent) relaxation rate is increased compared to the rate at longer TI, and this is dependent on pulse type. Between 7 and 64 ms after the inversion, rates in excess of 2 s^{-1} are observed for the lowest energy pulse (6.9 ms composite pulse), which is about twice the rate observed at the long TI's in our experiments, and in previously published work (Rooney, Johnson et al. 2007). This observed behavior is consistent with the notion that the decay for the shorter TI's is accelerated by the initially large difference in MP and WP magnetization ($S_{MP}(0) \ll S_{WP}(0)$), resulting in strong MT effects. This is further exemplified in Fig. 5, showing IR data from the corpus callosum ROI together with single- and bi-exponential fits. A clear deviation from single exponential relaxation is observed at short TI, which again is strongest for the lowest energy inversion pulse and high field (7 T). The vertical offset of the curves is attributed to variable WP inversion efficiency, which is particularly pronounced at 7 T (see Table 1 for estimated inversion efficiency).

Further analysis focused on two-pool model fitting based on the procedures outlined in Figs. 1 and 2. First, bi-exponential fitting was performed to the MT and inversion data (Step 1 in Fig. 1). An example of the extracted values for amplitudes (a_1 and a_2) and rates ((λ_1 and λ_2) of the two exponential components is shown in Fig. 6. The relative values of a_1 and a_2 varied strongly with inversion pulse type, with that of the rapidly relaxing component a_1 increasing with lower pulse energy. This was particularly apparent in WM, consistent with its higher MP fraction. The slowly relaxing component amplitude (a_2) varied little over the brain, indicating an efficient inversion. Exceptions were areas of in the posterior brain, attributed to off-resonance effects.

Figs. 7a and b illustrate the extraction of global $R_{1,MP}$ and $R_{1,WP}$ values based on constraints on $S_{MP}(0)$, for 3 T and 7 T data respectively (see also Fig. 1). Maximizing the number of voxels satisfying this constraint (indicate by the shaded area in the top right corner of each figure) led to an $R_{1,MP}$ estimate of 4.0 s^{-1} and 2.0 s^{-1} at 3 T and 7 T respectively, while

Author Manuscript Author Manuscript Author Manuscript Author Manuscript

$R_{1,WP}$ values were 0.40 s^{-1} and 0.35 s^{-1}. Based on the sensitivity of the $S_{MP}(0)$ distribution to changes in the $R_{1,MP}$ value, the $R_{1,MP}$ error margin can be estimated to be about 10%, while that for $R_{1,WP}$ was estimated at 20%.

Quantitative results of bi-exponential fitting and parameter extraction based on the ROI-based analysis (outlined in Fig. 2) are summarized in Tables 1 and 2. Table 1 shows subject-averaged values for pulse type-dependent parameters a_1, a_2, $S_{MP}(0)$, and $S_{WP}(0)$, confirming the decreased $S_{MP}(0)$ and increased contribution of the rapidly relaxing component for low energy inversion pulses. This trend was strongest for the 7 T data, which is attributed to the lower $R_{1,MP}$ at this field strength. Subject- and ROI-averaged values for parameters considered common to all pulse types (i.e. λ_1, λ_2, $R_{1,MP}$, $R_{1,WP}$, k_{WM}, k_{MW} , and f) are shown in Table 2. As indicated above, $R_{1,MP}$ was taken from the voxel-wise analysis, whereas $R_{1,WP}$ was fine-tuned based on ROI-averaged signals. Changes in $R_{1,WP}$ with fine-tuning were within 20% of the original values. Note that although k and f values are expected to not depend on field strength, appreciable differences in k-values were observed. This suggests that the experimental data are not fully described by our model.

Results of the noise simulations that evaluated the stability of the fitted parameters are shown in Table 3. These results indicate a precision that was for most parameters about 3%, with 7 T data generally showing smaller values compared to 3 T data. Note that the precision of $R_{1,WP}$ in this analysis is substantially better than the margin estimated in the voxel-wise analysis (for estimation of the global values for $R_{1,MP}$ and $R_{1,WP}$). This suggests that the accuracy of $R_{1,WP}$ is limited by the accuracy of $R_{1,MP}$, rather than by the noise (or inter-subject variations, judging from the low SD over subjects reported in Table 2).

Simulations of finite TR (incomplete signal recover between repeated measurements) on extracted parameter values showed relatively minor effects (Table 4). Strongest effects were observed at 7 T, as expected based on the slower T_1 recovery. Finite TR resulted in an underestimation of λ_1, and an overestimation of λ_2. As a result $R_{1,WP}$ was overestimated, while k_{WM} was underestimated. Little effect on f was observed.

The presence of a second, rapidly relaxing component to T_1 relaxation can interfere with attempts to quantify T_1 relaxation based on the conventional assumption that the inversion recovery is single-exponential. This is particularly true at short TI, as is strikingly apparent from the instantaneous T_1 shown in Fig. 8. Therefore, when quantifying T_1 relaxation assuming single-exponential behavior, it may be advantageous to exclude the recovery at short TI. Simulations show that for T_1 to be within 95% of $1/\lambda_2$ (i.e. for the instantaneous T_1 to stabilize), the minimum TI would need to be between 176 and 299 ms at 3 T, and between 324 and 443 ms at 7 T, with lower and upper values reflecting maximal and minimal MP saturation respectively.

DISCUSSION

The experiments described in this work demonstrate a dependence of IR on the parameters of the RF inversion pulse. Specifically, a bi-exponential recovery was observed, in which the amplitude of the rapid component depended on the power of the RF pulse. This finding

Author Manuscript Author Manuscript Author Manuscript Author Manuscript

is consistent with the notion that this component originates from MT between WP and MP, whose magnetization difference resulting from the inversion pulse is expected to depend on RF pulse energy. Simulations of the effects of the inversion pulses used in this work indeed indicated a highly variable magnetization difference between WP and MP. Importantly, the observed bi-exponential relaxation could be explained without considering multiple water compartments, including e.g. myelin water on one hand, and axonal water and interstitial water on the other. These compartments previously have been found do have distinct T_2 and/or T_2* relaxation characteristics (MacKay, Laule et al. 2006, Sati, van Gelderen et al. 2013), and in myelinated tissue of the trigeminal nerve, this may also be the case for T_1 relaxation (Does and Gore 2002). While in CNS white matter, exchange of myelin water with the other water compartments may be slow enough to have it contribute a distinct component to the IR curve (Kalantari, Laule et al. 2011), this does not explain the bi-exponentiality presented here, as our TE values were too long to have myelin water (T_2* < 20 ms) contribute substantially.

Previous studies have recognized the potential contribution of MT to bi-exponential signal recovery after inversion of WP magnetization, and were able to explain experimental IR data with a two-pool model of MT between WP (Gochberg, Kennan et al. 1997, Gochberg, Kennan et al. 1999, Prantner, Bretthorst et al. 2008, Labadie, Lee et al. 2014). The RF energy dependence of the recovery observed in the current study further solidifies this notion. In addition, the analysis presented here further characterizes the contribution of MT by comparing inversion recovery data with MT data. Use of the known MP saturation resulting from the MT pulse, and assuming $R_{1,MP}$ and $R_{1,WP}$ constant over the brain, allowed full characterization of MP and WP magnetization recovery and extraction of the two-pool model parameters. The resulting estimates for f in corpus callosum were, as expected, virtually identical for 3T and 7 T (0.266 versus 0.268) and consistent with what would be expected based on the close to 30% fraction of proteins and lipids (and hence an approximately MP fraction of 30%, considering that the hydrogen proton fraction in proteins and lipids is similar to that in water) (Randall 1938, Fatouros and Marmarou 1999). Our estimates furthermore appear consistent with previous MRI measurements of proton density not relying on MT contrast, which found WM water content to be around 70% (Volz, Noth et al. 2012, Volz, Noth et al. 2012, Mezer, Yeatman et al. 2013, Abbas, Gras et al. 2015). Nevertheless, our estimate of f is substantially higher than previous MT studies (Davies, Tozer et al. 2004, Sled, Levesque et al. 2004, Yarnykh and Yuan 2004, Stanisz, Odrobina et al. 2005, Yarnykh, Bowen et al. 2015). While this may, in part, be due to incorrect values for $R_{1,MP}$ assumed in these studies (Helms and Hagberg 2009), and their different approach for MT contrast generation, the reasons for this discrepancy remain poorly understood and require further investigation.

In this study, significant efforts were made towards estimation of $R_{1,MP}$, because of its importance in quantification of MT and T_1 relaxation. In our approach, both $R_{1,MP}$ and $R_{1,WP}$ and were assumed to be constant over the brain, which likely is inaccurate considering the diversity in molecular structure in brain tissues and the potential contribution of paramagnetic species (e.g. iron) to T_1. Nevertheless, our values of 4.0 and 2.0 s^{-1} for $R_{1,MP}$ at 3 T and 7 T respectively are in the range of average values of between

Author Manuscript Author Manuscript Author Manuscript Author Manuscript

2–5 s^{-1} reported for membrane model systems at fields from 8 T down to 1 T (Chan, Feigenson et al. 1971, Cornell, Pope et al. 1974, Deese, Dratz et al. 1982) or 2.3–6 s^{-1} derived from the dependence of R_1 on f at fields ranging from 7 T down to to 1.5 T (Gelman, Ewing et al. 2001, Rooney, Johnson et al. 2007, Helms and Hagberg 2009, Mezer, Yeatman et al. 2013, Callaghan, Helms et al. 2015).

Among the parameters extracted with the presented analysis is k_{WM} (and related parameter k_{MW}) representing the MT rate between WP and MP. Values of between 2.4 and 2.0 s^{-1} were found in the corpus callosum ROI at 3 T and 7 T respectively, which is on the low end of the 2.5–4 s^{-1} range reported in literature (Sled, Levesque et al. 2004, Yarnykh and Yuan 2004, Samsonov, Alexander et al. 2012, Dortch, Moore et al. 2013). In part, this may be related to methodological differences. In this regard, it should also be noted that k_{WM} represents an aggregate of processes that may contribute in varying amount between different methods: these include spin diffusion (Schuh, Banerjee et al. 1982, Ellena, Hutton et al. 1985), MT between MP and WP in myelin water, and MT between myelin water and water in other compartments. This may also explain the (small) differences seen in our 3 T and 7 T values. A slight underestimation of k_{WM} also appeared likely resultant from the finite TR used in our experiments (Table 4).

The finding of a bi-exponential T_1 recovery and its origin in MT effects has important implications for T_1-weighted MRI, in particular when reproducible contrast and accurate recovery rates are required. Bi-exponential fitting of MRI data acquired at a number of TI values would be one way to address this issue. As demonstrated above, this leads to T_1 estimates (from the slow component, i.e. λ_2^{-1}) in corpus callosum white matter of 905±27ms and 1293±28ms for 3 T and 7 T respectively (See Table 1), which both are somewhat higher than reported previously (for overview see (Rooney, Johnson et al. 2007)). However, this type of fitting is notoriously difficult to do, as signal to noise ratio is often limited and only few TI values are sampled. Fortunately, in human brain, the rate constants (λ_1, λ_2) differ substantially, with λ_1 being much higher than λ_2. Thus, at TI values much larger than λ_1^{-1}, the recovery can be characterized by a single-exponential function with rate constant λ_2, which then can be interpreted as an apparent R_1 value. This is further illustrated in the simulations shown in Fig. 8, indicating the minimum TI values at which the apparent (instantaneous) T_1 becomes independent of TI. This conclusion was also reached in a very recent paper investigation bi-exponential relaxation (Rioux, Levesque et al. 2015). The effects of bi-exponential relaxation in IR experiments can be further minimized by the use of high power adiabatic inversions that fully invert WP and fully saturate MP. Under this condition, contribution of the fast component is smallest and least variable. In alternative (non-IR) techniques for T_1 quantification, such as DESPOT1 (Deoni, Peters et al. 2005), MT may be a confound (Ou and Gochberg 2008), and its contribution will depend on experimental parameters.

In addition to affecting quantification, variable MP saturation can have influence on the contrast in T_1-weighted MRI and techniques that use inversion pulses for tissue suppression, and these effects extend beyond TI times indicated above (i.e. around 300 and 440 ms for worst cases, i.e. minimal MP saturation at 3 T and 7 T respectively). Examples of the latter are the use of double inversion recovery to selectively image grey or white matter (Redpath

Author Manuscript Author Manuscript Author Manuscript Author Manuscript

and Smith 1994), IR based myelin imaging using ViSTa (Oh, Bilello et al. 2013). For consistent results, optimization of TI values ideally would take into account the power of the RF inversion pulse. As shown in Fig. 3d, the zero crossing of the IR curves depends on the MP saturation level and therefore on the applied RF energy. Of course, such optimization would not be sufficient to account for variations in *f*.

As indicated above, the contribution of the rapidly relaxing component to the inversion recovery is, aside from *f*, dependent on RF pulse parameters, and field strength. The latter dependence originates from the effect of field strength on $R_{1,MP}$: a_1 increases with decreases in $R_{1,MP}$ at higher field in the complicated fashion indicated by equations (1–4). Thus, at fields above 7 T, contribution of the fast component should further increase. Together with the increase in SNR available at high field, this would improve determination of a_1, a_2, λ_1, and λ_2, and potentially allow robust quantification of MT exchange rates (k_{MF} and k_{WF}) from IR data only, without the need for dedicated MT experiments. Conversely, at 1.5 T, the deviation from single-exponential inversion recovery is expected to be smaller.

Although our analysis of T_1 relaxation assumed a dominant contribution from MT, it should be realized that in some brain regions, paramagnetic species such as iron may contribute as well. For example, in the iron-rich grey matter of the globus pallidus, this may increase the relaxation rate by as much as 0.3 s^{-1} at 7 T (Rooney, Johnson et al. 2007). This complicates the extraction of parameters such as *f* and k_{WM} from the bi-exponential fit, which may require additional information (e.g. estimates of local iron content based on R_2* data).

A few limitations of the current study deserve further attention. One limitation is the assumed efficiency of MT pulses, which was based on experimental variation of pulse duration. This implicitly assumed a narrow distribution of T_2 values for the MP pool. However, it is possible that a fraction of MPs escape saturation, due to an either very short or very long T_2. This would then lead to an underestimation of *f*. Judged from the similarity between fitted R_{1WP} found by either assuming fixed MT efficiency (in the ROI analysis) or fixed (global) $R_{1,WP}$ (in the voxel-wise analysis), this appeared not to be a major issue. Another limitation is the sensitivity of multi-exponential fitting and parameter extraction to measurement noise. The SD value of some of the ROI-derived parameters reached 5% even is the presence of a high (500:1) SNR. This is attributed to the inherent difficulty of the fitting problem, combined with temporal instabilities (caused by e.g. head motion). Finally, the limited accuracy of the R_{1MP} value also limits the accuracy in other derived parameters, in particular R_{1WP} and the k_{MW}.

CONCLUSION

Joint analysis of IR and MT experiments in the human brain further solidifies the notion that bi-exponential IR originates from MT effects, and shows that the relative magnitude of the two exponentials depends on the details of the RF inversion pulse. Proper interpretation and reproducible quantification with a two-pool model of magnetization transfer required proper estimates of the T_1s of macromolecular and water protons.

Author Manuscript Author Manuscript Author Manuscript Author Manuscript

Acknowledgments

This work has been supported by the Intramural program of NINDS.

References

Abbas Z, Gras V, Mollenhoff K, Oros-Peusquens AM, Shah NJ. Quantitative water content mapping at clinically relevant field strengths: a comparative study at 1.5 T and 3 T. Neuroimage. 2015; 106:404–413. [PubMed: 25463455]

Barazany D, Assaf Y. Visualization of cortical lamination patterns with magnetic resonance imaging. Cereb Cortex. 2012; 22(9):2016–2023. [PubMed: 21983231]

Barral JK, Gudmundson E, Stikov N, Etezadi-Amoli M, Stoica P, Nishimura DG. A robust methodology for in vivo T1 mapping. Magn Reson Med. 2010; 64(4):1057–1067. [PubMed: 20564597]

Callaghan MF, Helms G, Lutti A, Mohammadi S, Weiskopf N. A general linear relaxometry model of R1 using imaging data. Magn Reson Med. 2015; 73(3):1309–1314. [PubMed: 24700606]

Chan SI, Feigenson GW, Seiter CH. Nuclear relaxation studies of lecithin bilayers. Nature. 1971; 231(5298):110–112. [PubMed: 16062576]

Clark VP, Courchesne E, Grafe M. In vivo myeloarchitectonic analysis of human striate and extrastriate cortex using magnetic resonance imaging. Cereb Cortex. 1992; 2(5):417–424. [PubMed: 1422094]

Constable RT, Smith RC, Gore JC. Signal-to-noise and contrast in fast spin echo (FSE) and inversion recovery FSE imaging. J Comput Assist Tomogr. 1992; 16(1):41–47. [PubMed: 1729305]

Cornell BA, Pope JM, Troup GJ. A pulsed N.M.R study of D2O bound to 1,2 dipalmitoyl phosphatidylcholine. Chem Phys Lipids. 1974; 13(2):183–201. [PubMed: 4430062]

Davies GR, Tozer DJ, Cercignani M, Ramani A, Dalton CM, Thompson AJ, Barker GJ, Tofts PS, Miller DH. Estimation of the macromolecular proton fraction and bound pool T2 in multiple sclerosis. Mult Scler. 2004; 10(6):607–613. [PubMed: 15584482]

Deese AJ, Dratz EA, Hymel L, Fleischer S. Proton NMR T1, T2, and T1 rho relaxation studies of native and reconstituted sarcoplasmic reticulum and phospholipid vesicles. Biophys J. 1982; 37(1): 207–216. [PubMed: 6459803]

Deese AJ, Dratz EA, Hymel L, Fleischer S. Proton Nmr T1, T2, and T1-Rho Relaxation Studies of Native and Reconstituted Sarcoplasmic-Reticulum and Phospholipid-Vesicles. Biophysical Journal. 1982; 37(1):207–216. [PubMed: 6459803]

Deoni SC, Peters TM, Rutt BK. High-resolution T1 and T2 mapping of the brain in a clinically acceptable time with DESPOT1 and DESPOT2. Magn Reson Med. 2005; 53(1):237–241. [PubMed: 15690526]

Deoni SC, Rutt BK, Arun T, Pierpaoli C, Jones DK. Gleaning multicomponent T1 and T2 information from steady-state imaging data. Magn Reson Med. 2008; 60(6):1372–1387. [PubMed: 19025904]

Dinse J, Hartwich N, Waehnert MD, Tardif CL, Schafer A, Geyer S, Preim B, Turner R, Bazin PL. A cytoarchitecture-driven myelin model reveals area-specific signatures in human primary and secondary areas using ultra-high resolution in-vivo brain MRI. Neuroimage. 2015

Dinse J, Waehnert M, Tardif CL, Schafer A, Geyer S, Turner R, Bazin PL. A histology-based model of quantitative T1 contrast for in-vivo cortical parcellation of high-resolution 7 Tesla brain MR images. Med Image Comput Comput Assist Interv. 2013; 16(Pt 2):51–58. [PubMed: 24579123]

Does MD, Gore JC. Compartmental study of T(1) and T(2) in rat brain and trigeminal nerve in vivo. Magn Reson Med. 2002; 47(2):274–283. [PubMed: 11810670]

Dortch RD, Moore J, Li K, Jankiewicz M, Gochberg DF, Hirtle JA, Gore JC, Smith SA. Quantitative magnetization transfer imaging of human brain at 7 T. Neuroimage. 2013; 64:640–649. [PubMed: 22940589]

Du J, Sheth V, He Q, Carl M, Chen J, Corey-Bloom J, Bydder GM. Measurement of T1 of the ultrashort T2* components in white matter of the brain at 3T. PLoS One. 2014; 9(8):e103296. [PubMed: 25093859]

Author Manuscript Author Manuscript Author Manuscript Author Manuscript

Edzes HT, Samulski ET. Cross relaxation and spin diffusion in the proton NMR or hydrated collagen. Nature. 1977; 265(5594):521–523. [PubMed: 834303]

Ellena JF, Hutton WC, Cafiso DS. Elucidation of Cross-Relaxation Pathways in Phospholipid-Vesicles Utilizing Two-Dimensional H-1-Nmr Spectroscopy. Journal of the American Chemical Society. 1985; 107(6):1530–1537.

Fatouros PP, Marmarou A. Use of magnetic resonance imaging for in vivo measurements of water content in human brain: method and normal values. J Neurosurg. 1999; 90(1):109–115. [PubMed: 10413163]

Fatouros PP, Marmarou A, Kraft KA, Inao S, Schwarz FP. In vivo brain water determination by T1 measurements: effect of total water content, hydration fraction, and field strength. Magn Reson Med. 1991; 17(2):402–413. [PubMed: 2062213]

Gelman N, Ewing JR, Gorell JM, Spickler EM, Solomon EG. Interregional variation of longitudinal relaxation rates in human brain at 3.0 T: relation to estimated iron and water contents. Magn Reson Med. 2001; 45(1):71–79. [PubMed: 11146488]

Gochberg DF, Gore JC. Quantitative imaging of magnetization transfer using an inversion recovery sequence. Magn Reson Med. 2003; 49(3):501–505. [PubMed: 12594753]

Gochberg DF, Kennan RP, Gore JC. Quantitative studies of magnetization transfer by selective excitation and T1 recovery. Magn Reson Med. 1997; 38(2):224–231. [PubMed: 9256101]

Gochberg DF, Kennan RP, Robson MD, Gore JC. Quantitative imaging of magnetization transfer using multiple selective pulses. Magn Reson Med. 1999; 41(5):1065–1072. [PubMed: 10332891]

Helms G, Hagberg GE. In vivo quantification of the bound pool T1 in human white matter using the binary spin-bath model of progressive magnetization transfer saturation. Phys Med Biol. 2009; 54(23):N529–540. [PubMed: 19904029]

Horch RA, Gore JC, Does MD. Origins of the ultrashort-T2 1H NMR signals in myelinated nerve: a direct measure of myelin content? Magn Reson Med. 2011; 66(1):24–31. [PubMed: 21574183]

Kalantari S, Laule C, Bjarnason TA, Vavasour IM, MacKay AL. Insight into in vivo magnetization exchange in human white matter regions. Magnetic resonance in medicine : official journal of the Society of Magnetic Resonance in Medicine / Society of Magnetic Resonance in Medicine. 2011; 66(4):1142–1151.

Kingsley PB, Ogg RJ, Reddick WE, Steen RG. Correction of errors caused by imperfect inversion pulses in MR imaging measurement of T1 relaxation times. Magn Reson Imaging. 1998; 16(9): 1049–1055. [PubMed: 9839989]

Koenig SH, Brown RD 3rd, Spiller M, Lundbom N. Relaxometry of brain: why white matter appears bright in MRI. Magn Reson Med. 1990; 14(3):482–495. [PubMed: 2355830]

Labadie C, Lee JH, Rooney WD, Jarchow S, Aubert-Frecon M, Springer CS Jr, Moller HE. Myelin water mapping by spatially regularized longitudinal relaxographic imaging at high magnetic fields. Magn Reson Med. 2014; 71(1):375–387. [PubMed: 23468414]

MacKay A, Laule C, Vavasour I, Bjarnason T, Kolind S, Madler B. Insights into brain microstructure from the T2 distribution. Magnetic resonance imaging. 2006; 24(4):515–525. [PubMed: 16677958]

Marques JP, Kober T, Krueger G, van der Zwaag W, Van de Moortele PF, Gruetter R. MP2RAGE, a self bias-field corrected sequence for improved segmentation and T1-mapping at high field. Neuroimage. 2010; 49(2):1271–1281. [PubMed: 19819338]

Mezer A, Yeatman JD, Stikov N, Kay KN, Cho NJ, Dougherty RF, Perry ML, Parvizi J, Hua le H, Butts-Pauly K, Wandell BA. Quantifying the local tissue volume and composition in individual brains with magnetic resonance imaging. Nat Med. 2013; 19(12):1667–1672. [PubMed: 24185694]

Mugler JP 3rd, Brookeman JR. Three-dimensional magnetization-prepared rapid gradient-echo imaging (3D MP RAGE). Magn Reson Med. 1990; 15(1):152–157. [PubMed: 2374495]

Oh SH, Bilello M, Schindler M, Markowitz CE, Detre JA, Lee J. Direct visualization of short transverse relaxation time component (ViSTa). Neuroimage. 2013; 83C:485–492. [PubMed: 23796545]

Author Manuscript Author Manuscript Author Manuscript Author Manuscript

Ordidge RJ, Gibbs P, Chapman B, Stehling MK, Mansfield P. High-speed multislice T1 mapping using inversion-recovery echo-planar imaging. Magn Reson Med. 1990; 16(2):238–245. [PubMed: 2266843]

Ou X, Gochberg DF. MT effects and T1 quantification in single-slice spoiled gradient echo imaging. Magn Reson Med. 2008; 59(4):835–845. [PubMed: 18302249]

Prantner AM, Bretthorst GL, Neil JJ, Garbow JR, Ackerman JJ. Magnetization transfer induced biexponential longitudinal relaxation. Magn Reson Med. 2008; 60(3):555–563. [PubMed: 18759367]

Randall LO. Chemical topography of the brain. Journal of Biological Chemistry. 1938; 124(2):0481–0488.

Redpath TW, Smith FW. Technical note: use of a double inversion recovery pulse sequence to image selectively grey or white brain matter. Br J Radiol. 1994; 67(804):1258–1263. [PubMed: 7874427]

Rioux JA, Levesque IR, Rutt BK. Biexponential longitudinal relaxation in white matter: Characterization and impact on T mapping with IR-FSE and MP2RAGE. Magn Reson Med. 2015

Rooney WD, Johnson G, Li X, Cohen ER, Kim SG, Ugurbil K, Springer CS Jr. Magnetic field and tissue dependencies of human brain longitudinal 1H2O relaxation in vivo. Magn Reson Med. 2007; 57(2):308–318. [PubMed: 17260370]

Samsonov A, Alexander AL, Mossahebi P, Wu YC, Duncan ID, Field AS. Quantitative MR imaging of two-pool magnetization transfer model parameters in myelin mutant shaking pup. Neuroimage. 2012; 62(3):1390–1398. [PubMed: 22664569]

Sati P, van Gelderen P, Silva AC, Reich DS, Merkle H, de Zwart JA, Duyn JH. Micro-compartment specific T2() relaxation in the brain. Neuroimage. 2013; 77:268–278. [PubMed: 23528924]

Schuh JR, Banerjee U, Muller L, Chan SI. The phospholipid packing arrangement in small bilayer vesicles as revealed by proton magnetic resonance studies at 500 MHz. Biochim Biophys Acta. 1982; 687(2):219–225. [PubMed: 7093252]

Sled JG, Levesque I, Santos AC, Francis SJ, Narayanan S, Brass SD, Arnold DL, Pike GB. Regional variations in normal brain shown by quantitative magnetization transfer imaging. Magnetic resonance in medicine : official journal of the Society of Magnetic Resonance in Medicine / Society of Magnetic Resonance in Medicine. 2004; 51(2):299–303.

Sled JG, Levesque I, Santos AC, Francis SJ, Narayanan S, Brass SD, Arnold DL, Pike GB. Regional variations in normal brain shown by quantitative magnetization transfer imaging. Magn Reson Med. 2004; 51(2):299–303. [PubMed: 14755655]

Smith RC, Constable RT, Reinhold C, McCauley T, Lange RC, McCarthy S. Fast spin echo STIR imaging. J Comput Assist Tomogr. 1994; 18(2):209–213. [PubMed: 8126269]

Stanisz GJ, Odrobina EE, Pun J, Escaravage M, Graham SJ, Bronskill MJ, Henkelman RM. T1, T2 relaxation and magnetization transfer in tissue at 3T. Magn Reson Med. 2005; 54(3):507–512. [PubMed: 16086319]

Stikov N, Boudreau M, Levesque IR, Tardif CL, Barral JK, Pike GB. On the accuracy of T1 mapping: searching for common ground. Magn Reson Med. 2015; 73(2):514–522. [PubMed: 24578189]

Stuber C, Morawski M, Schafer A, Labadie C, Wahnert M, Leuze C, Streicher M, Barapatre N, Reimann K, Geyer S, Spemann D, Turner R. Myelin and iron concentration in the human brain: a quantitative study of MRI contrast. Neuroimage. 2014; 93(Pt 1):95–106. [PubMed: 24607447]

Tannus A, Garwood M. Adiabatic pulses. NMR Biomed. 1997; 10(8):423–434. [PubMed: 9542739]

Van Gelderen, P.; Koretsky, AP.; de Zwart, JA.; Duyn, JH. A simple B1 correction method for high resolution neuroimaging. Proceedings, 14th scientific meeting ISMRM; Seattle,WA. 2006. p. 2355

Volz S, Noth U, Deichmann R. Correction of systematic errors in quantitative proton density mapping. Magn Reson Med. 2012; 68(1):74–85. [PubMed: 22144171]

Volz S, Noth U, Jurcoane A, Ziemann U, Hattingen E, Deichmann R. Quantitative proton density mapping: correcting the receiver sensitivity bias via pseudo proton densities. Neuroimage. 2012; 63(1):540–552. [PubMed: 22796988]

Wilhelm MJ, Ong HH, Wehrli SL, Li C, Tsai PH, Hackney DB, Wehrli FW. Direct magnetic resonance detection of myelin and prospects for quantitative imaging of myelin density. Proceedings of the National Academy of Sciences of the United States of America. 2012; 109(24): 9605–9610. [PubMed: 22628562]

Author Manuscript Author Manuscript Author Manuscript Author Manuscript

Yarnykh VL, Bowen JD, Samsonov A, Repovic P, Mayadev A, Qian P, Gangadharan B, Keogh BP, Maravilla KR, Jung Henson LK. Fast Whole-Brain Three-dimensional Macromolecular Proton Fraction Mapping in Multiple Sclerosis. Radiology. 2015; 274(1):210–220. [PubMed: 25208343]

Yarnykh VL, Yuan C. Cross-relaxation imaging reveals detailed anatomy of white matter fiber tracts in the human brain. Neuroimage. 2004; 23(1):409–424. [PubMed: 15325389]

Zhu DC, Penn RD. Full-brain T1 mapping through inversion recovery fast spin echo imaging with time-efficient slice ordering. Magn Reson Med. 2005; 54(3):725–731. [PubMed: 16086307]

Zimmerman JR, Britten WE. Nuclear magnetic resonance studies in multiple phase sysems: lifetime of a water molecule in an adsorbing phase on silica gel. J Phys Chem. 1957; 61:1328–1333.

Author Manuscript Author Manuscript Author Manuscript Author Manuscript

Highlights

- MRI T_1 contrast to study brain anatomy depends on experimental details - Variability is introduced by the type of RF inversion pulse used
- It can be attributed to the magnetization level of macromolecular protons
- It can be minimized by using long inversion times and high RF power
- Proper modeling of this effect allows quantification of tissue parameters

Author Manuscript Author Manuscript Author Manuscript Author Manuscript

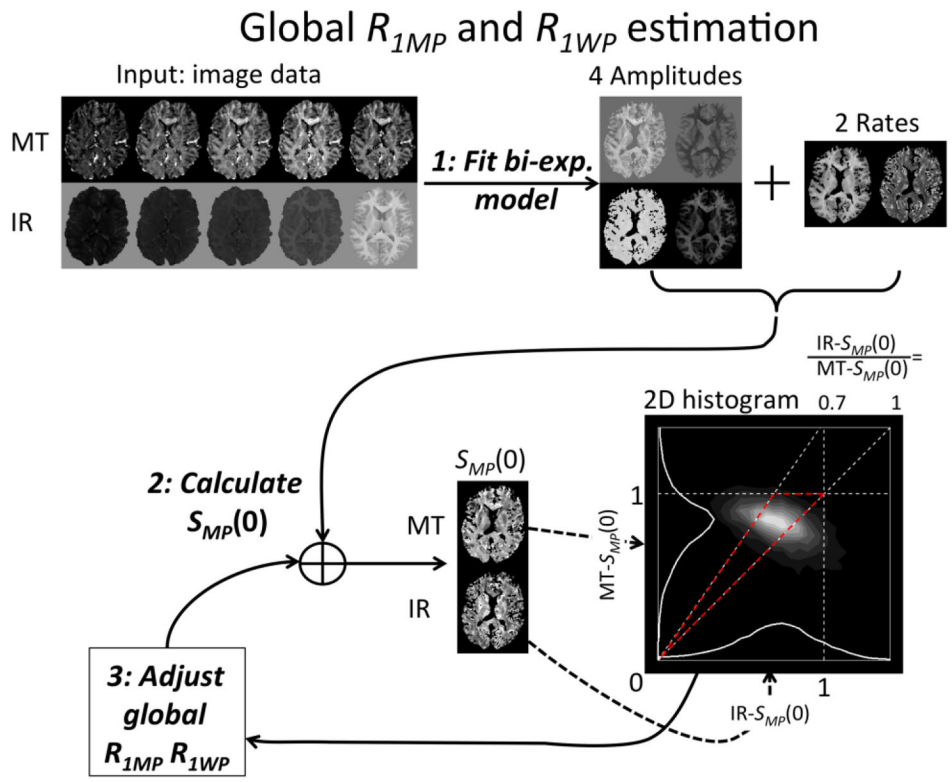

Figure 1.

Voxel-wise fitting and parameter extraction to derive global $R_{1,MP}$ and $R_{1,WP}$ estimates. First (step 1) is the combined fitting of bi-exponential model to data from MT experiment and a single (A5.1 pulse) IR experiment. In step 2, $S_{MP}(0)$ values are calculated for both experiments based on global values for $R_{1,MP}$ and $R_{1,wP}$. Then (step 3) R_1 values are adjusted iteratively (repeating step 2) to maximize the fraction of voxels with $S_{MP}(0)$ values within in the expected boundaries, outlined by the red triangle.

Author Manuscript Author Manuscript Author Manuscript Author Manuscript

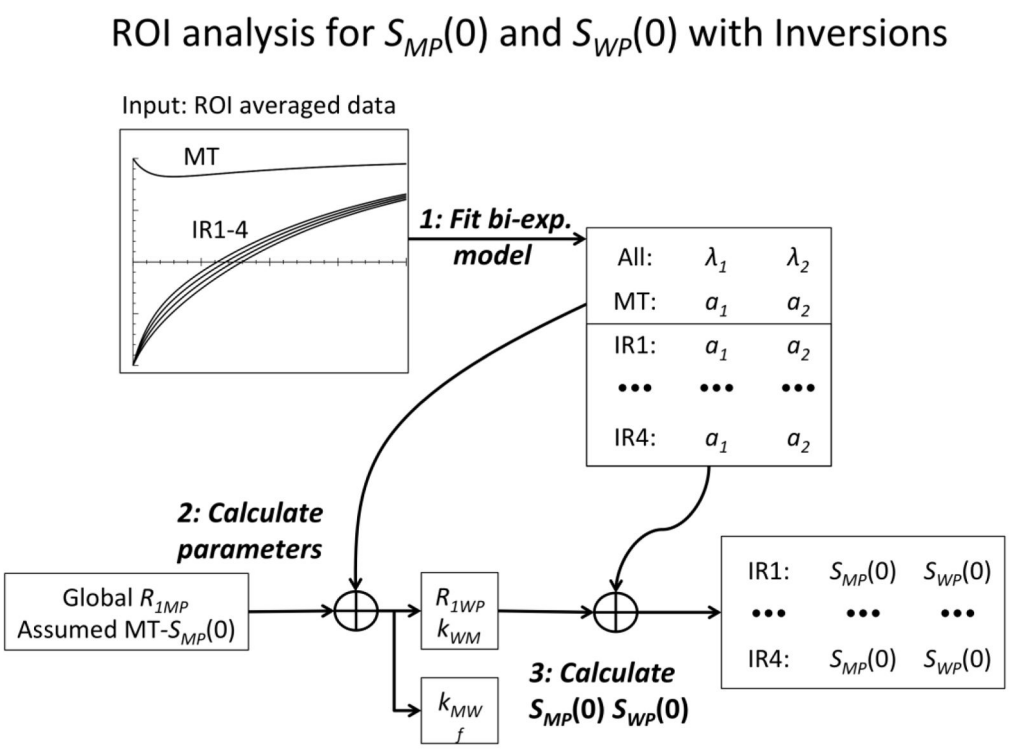

Figure 2.

ROI-based fitting and calculation of $S_{MP}(0)$ and $S_{WP}(0)$ for IR data. First, (step 1), ROI-averaged data from MT experiment and IR experiments with four different inversion pulses are fitted to the bi-exponential model, resulting one set of λ's and 5 sets of values for a_1 and a_2. Then (step 2), based on global $R_{1,MP}$ from voxel-wise analysis (see Fig. 1), and assumed $S_{MP}(0)$ for MT experiment, the MT parameters extracted in step 1 are used to calculate R_{1WP}, k_{WM}, k_{MW} and f. Then, in step 3, R_{1WP}, and k_{WM} are combined with the IR a's and λ's from step 1 to calculate the $S_{MP}(0)$ and $S_{WP}(0)$ for each IR experiment.

Author Manuscript Author Manuscript Author Manuscript Author Manuscript

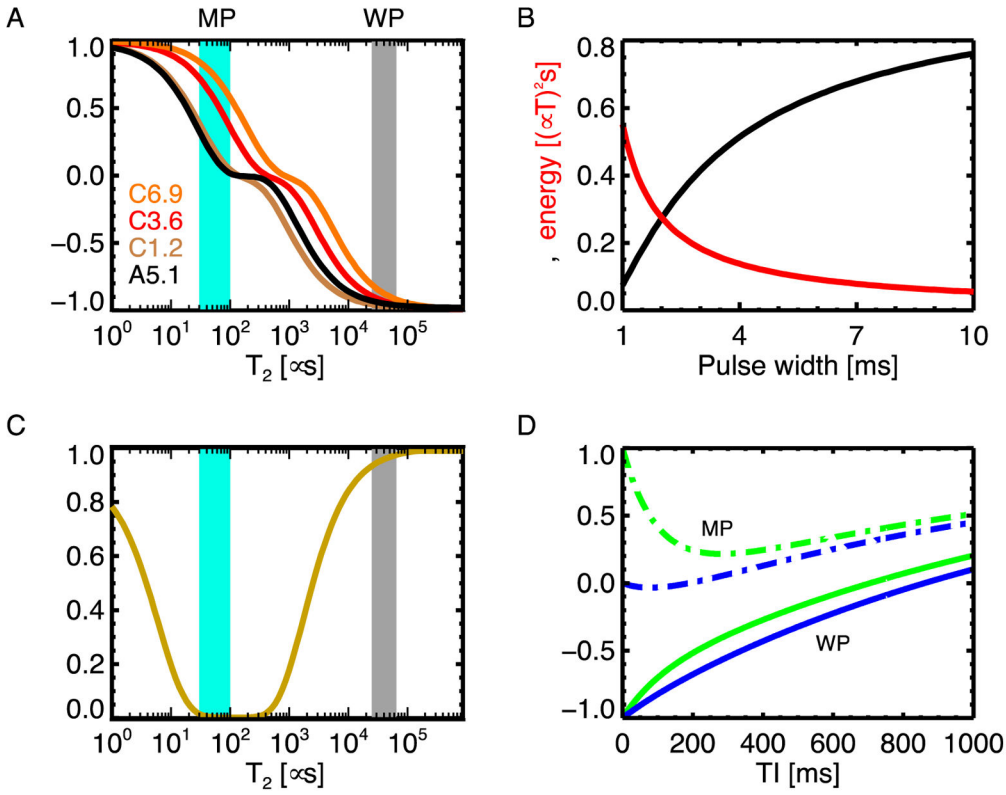

Figure 3.

Simulated effect of IR pulses (a,b,d) and MT pulse (c) on longitudinal magnetization (M). **A**: Effect of inversion pulse on M as a function of T_2. While different inversion pulse types similarly invert long T_2 species characteristic of WP (grey band), they differentially affect the short T_2 MP (blue band). **B**: For MP (T_2 = 70μs), magnetization (black) after a composite inversion pulse and the latter's energy (red) depend strongly on pulse duration **C:** Effect of MT pulse on M as a function of T_2. Nearly complete saturation (M~0) is achieved for MP, while WPs are minimally affected. **D**: Calculated MP (dashed lines) and WP (solid lines) magnetization following inversion, as function of (TI) time, for two extreme cases: no MP saturation (green), and complete MP saturation (blue). Parameters for this simulation were taken from mean 7 T values of Table 2. Perfect WP inversion was assumed.

Author Manuscript Author Manuscript Author Manuscript Author Manuscript

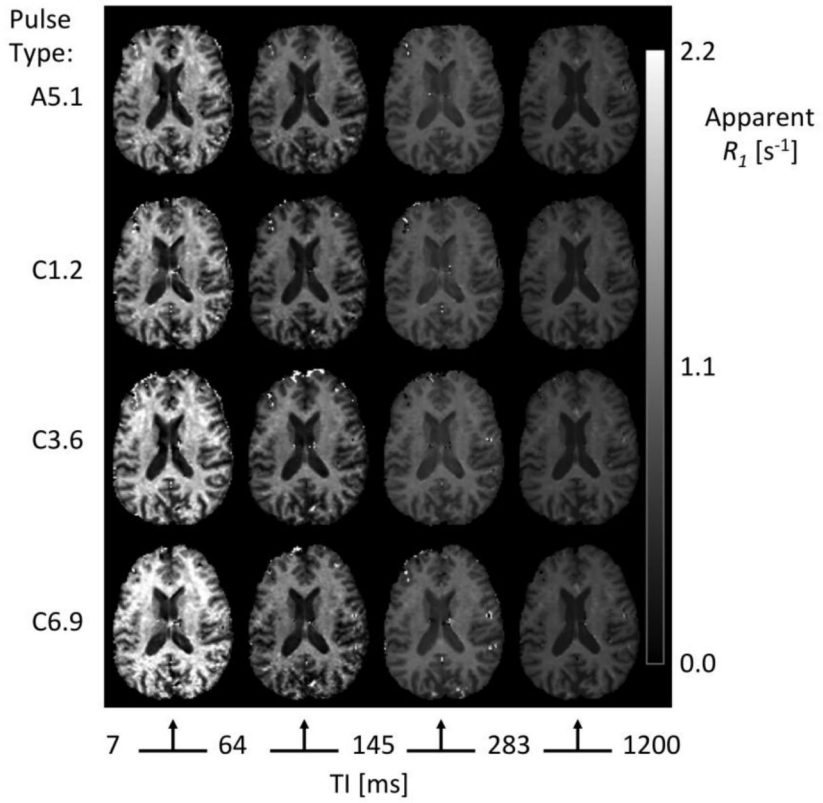

Figure 4.

Effect of inversion pulse type (rows) on apparent (instantaneous) R_1 (scale in seconds), at increasing TI (columns). Apparent R_1, as calculated from adjacent TI's, was highest for lowest power composite pulse (C6.9) and short TI.

Author Manuscript Author Manuscript Author Manuscript Author Manuscript

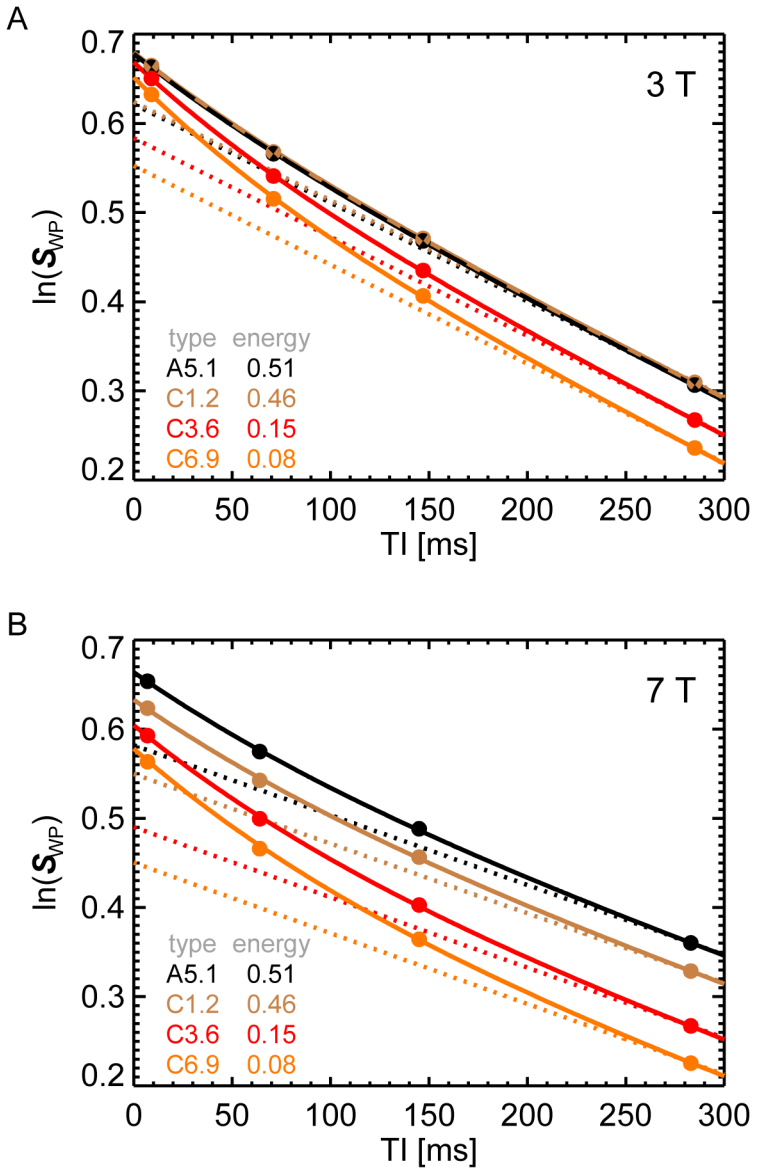

Figure 5.

Demonstration of bi-exponential IR, based on measured and fitted S_{WP} in corpus callosum ROIs at 3 T (**A**) and 7 T (**B**). Subject and ROI-averaged IR data are shown in range of 0–300ms, where strongest effects of the bi-exponential nature of the decay is observed. The dashed lines are the single-exponential fits to the two longest TI's (283 and 1200 ms). Deviation form linearity (i.e. from single-exponential behavior) is strongest at early TI's and low power pulses (C3.6 and C6.9) at 7 T. At 3 T, the adiabatic (A5.1) and shortest composite pulse (C1.2) produced virtually identical results.

Author Manuscript Author Manuscript Author Manuscript Author Manuscript

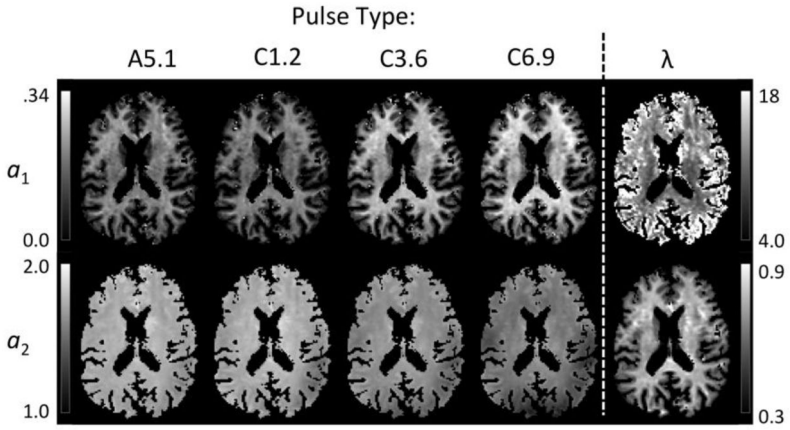

Figure 6.

Example of voxel-wise fitting of bi-exponential relaxation behavior. Shown are results for a single slice in a single subject at 7 T. The contribution of the fast component (represented by a_1) increases with increasing pulse length for composite pulses C1.2-C6.9 (decreasing energy). The voxels with CSF where masked out from the images, as their fits resulted in extreme values for some of the parameters due to a close to single-exponential nature of IR in CSF.

Author Manuscript Author Manuscript Author Manuscript Author Manuscript

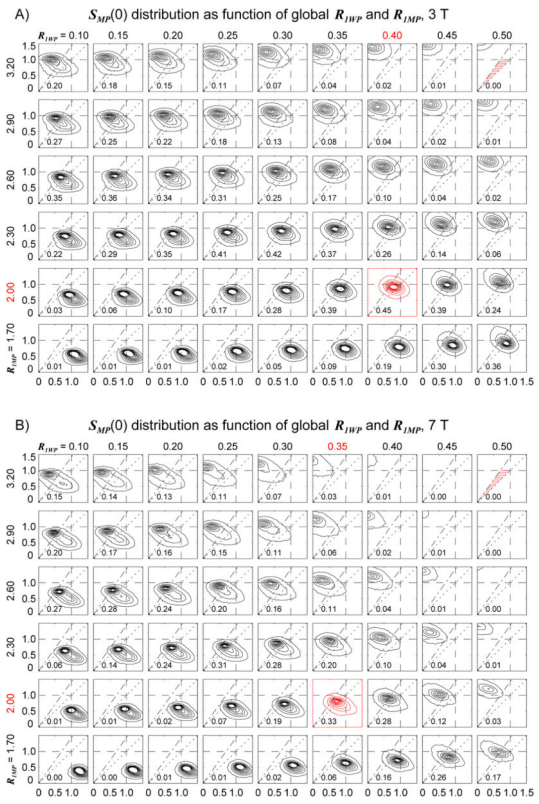

Figure 7.

Voxel-wise analysis approach to extract global values for $R_{1,WP}$ and $R_{1,MP}$. Contour plots of 2D histograms show the distribution of calculated $S_{MP}(0)$ values for IR (horizontal axis) and MT data (vertical axis). Histograms were calculated for a range of R_{1WP} and R_{1MP} values (columns and rows respectively, values in s^{-1}), and reflect all voxels in all subjects at 3 T and 7 T (**A** and **B** respectively). The dashed lines in each histogram show the range of expected $S_{MP}(0)$ values (both $S_{MP,Inv}(0)$ and $S_{MP,MT}(0)$ <1.0 and 0.7 < $S_{MP,Inv}(0)$ / $S_{MP,MT}(0)$ < 1.0; the area is indicated with shading in top right plots). The numbers printed in the plots are the fractions of the number of brain voxels falling within the expected range (see also Fig. 1). The histogram with the highest fraction (in red) was identified to deduce the appropriate values for $R_{1,WP}$ and $R_{1,MP}$ for each field strength.

Author Manuscript Author Manuscript Author Manuscript Author Manuscript

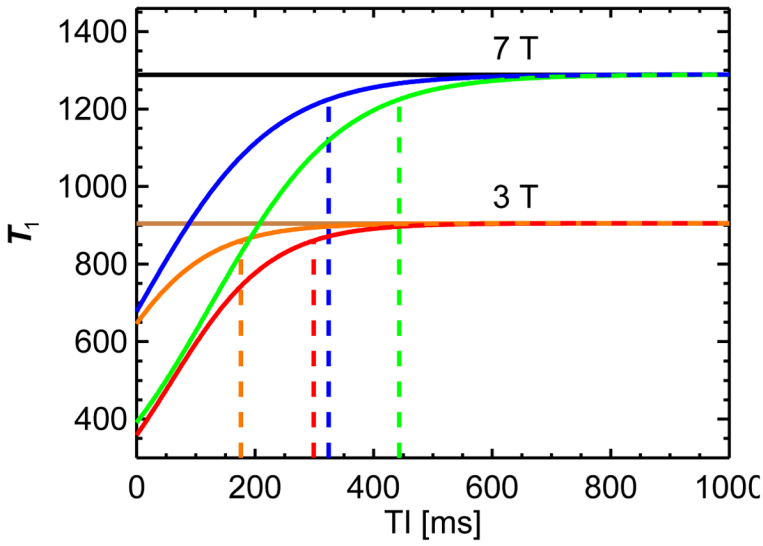

Figure 8.

The instantaneous $T_1\ (=-S(t)/(\frac{dS(t)}{dt}))$ calculated from two-pool model simulated data (using the average parameters from Table 2), for the minimum and maximum effects (high and low power inversion) (red/orange= 3 T, green/blue 7 T, orange/blue minimum effect, red/green maximum). The vertical lines indicate the minimum TI for an error smaller than 5% in the calculated (single-exponential) T_1.

Author Manuscript Author Manuscript Author Manuscript Author Manuscript

Table 1

Pulse-dependent results of two-pool fitting in corpus callosum white matter of IR experiments at 3 T and 7 T (n=10). Reported are subject averages (and SD's) of amplitudes (a_1 and a_2) and saturation levels assuming f =0.27 (based on MT data). Pulse energy is integral of $B_1{}^2$ in units of $(\mu T)^2 s$. Range indicates theoretically possible values for all possible effects of inversion pulse on MP, while assuming a 100% inversion of WP.

B_0	Type	Energy	a_1	a_2	S_{MP}	S_{WP}
3 T	A5.1	0.51	0.116 (0.009)	1.854 (0.008)	0.87	1.97
	C1.2	0.46	0.113 (0.010)	1.860 (0.009)	0.89	1.97
	C3.6	0.15	0.170 (0.011)	1.781 (0.011)	0.62	1.95
	C6.9	0.08	0.194 (0.013)	1.725 (0.015)	0.48	1.92
	range (theory)		0.08–0.30	1.92–1.71	0.0–1.0	
7 T	A5.1	0.51	0.173 (0.012)	1.769 (0.010)	0.87	1.94
	C1.2	0.46	0.170 (0.012)	1.714 (0.044)	0.84	1.88
	C3.6	0.15	0.225 (0.016)	1.605 (0.047)	0.56	1.83
	C6.9	0.08	0.245 (0.026)	1.538 (0.052)	0.46	1.78
	range (theory)		0.16–0.40	1.84–1.60	0.0–1.0	

Author Manuscript Author Manuscript Author Manuscript Author Manuscript

Table 2

The average (SD) of extracted two-pool model parameters (using Eq. 1–4) in corpus callosum ROI (n=10), $R_{1,MP}$ is reported without SD as a single value was assumed for all subjects; all rates are reported in s^{-1}.

B_0	λ_1	λ_2	f	$R_{1,WP}$	$R_{1,MP}$	k_{WM}	k_{MW}
3 T	12.11 (0.83)	1.103 (0.034)	0.265 (0.014)	0.410 (0.027)	4.0	2.39 (0.26)	6.61 (0.64)
7 T	9.25 (0.68)	0.773 (0.016)	0.268 (0.013)	0.406 (0.018)	2.0	2.04 (0.15)	5.58 (0.54)

Author Manuscript Author Manuscript Author Manuscript Author Manuscript

Table 3

Noise simulation results: the SD (absolute and relative percentage) of fitted and derived parameters for simulated data with baseline (ROI) SNR of 500 (based on the R^2 of the actual fit results), all rates are in units of s^{-1}.

B_0		a_1,a_2	λ_1	λ_2	f	$R_{1,WP}$	k_{WM}	k_{MW}	$S_{MP}(0)$
3 T	SD	0.0035	0.32	0.0025	0.0054	0.014	0.069	0.26	0.032
	%		2.8	0.23	2.7	3.5	3.3	4.6	3.2
7 T	SD	0.0035	0.21	0.0021	0.0036	0.0067	0.052	0.17	0.022
	%		2.3	0.25	1.8	1.9	2.5	3.0	2.2

Author Manuscript Author Manuscript Author Manuscript Author Manuscript

Table 4

Comparison the fitting results from simulations (based on the parameters printed in Table 2) run with the experimental TR and a TR four times as long, all rates are in units of s^{-1}.

B_0	TR	f	$R_{1,WP}$	k_{WM}	k_{MW}
3 T	12,9	0.271	0.363	2.39	6.45
	4,3	0.270	0.391	2.33	6.32
7 T	12,9	0.268	0.405	2.04	5.56
	4,3	0.262	0.455	1.85	5.21